Article

Electrocatalytic Efficiency Regulation Between Target-Induced HRP-Mimicking DNAzyme and GOx with Low Background for Ultrasensitive Detection of Thrombin

Lingqi Kong, Ding Wang, Ya-qin Chai, Yali Yuan, and Ruo Yuan

Anal. Chem., **Just Accepted Manuscript** • DOI: 10.1021/acs.analchem.9b02498 • Publication Date (Web): 26 Jun 2019

Electrocatalytic Efficiency Regulation Between Target-Induced HRP-Mimicking DNAzyme and GOx with Low Background for Ultrasensitive Detection of Thrombin

Lingqi Kong, Ding Wang, Yaqin Chai, Yali Yuan*, Ruo Yuan*

Key Laboratory of Luminescence and Real-Time Analytical Chemistry (Southwest University), Ministry of Education, College of Chemistry and Chemical Engineering, Southwest University, Chongqing 400715, People's Republic of China

* Corresponding author. Tel.: +86-23-68252277; Fax: +86-23-68253172

E-mail address: y198688@swu.edu.cn (Y. L. Yuan); yuanruo@swu.edu.cn (R. Yuan)

ABSTRACT

Herein, an efficient target-activated enzyme cascade electrocatalysis with low background signal was employed to establish electrochemical biosensor for ultrasensitive detection of thrombin *via* regulating electrocatalytic efficiency between target-induced hemin/G-quadruplex horseradish peroxidase-mimicking DNAzyme (HRP-mimicking DNAzyme) and glucose oxidase (GOx). Impressively, only when the target thrombin was introduced, the HRP-mimicking DNAzyme acting simultaneously as electrochemical signal probe would be formed to activate high-efficiency enzyme cascade electrocatalysis for reducing background signal significantly, which could overcome the defect of inevitable high background signal during the detection of target in the traditional cascade electrocatalysis of two existing bioenzymes. In addition, the detection sensitivity could be further improved by regulating the side length of rigid DNA tetrahedron (TDN) scaffold anchored HRP-mimicking DNAzyme and GOx at adjacent vertices for high enzyme cascade electrocatalytic efficiency. Consequently, the proposed biosensor demonstrated a low detection limit down to 0.3 fM for target thrombin, which provided a promising method for ultrasensitive monitoring of biomolecules in sensing analysis and disease diagnosis.

KEYWORDS: electrochemical biosensor; hemin/G-quadruplex DNAzyme; enzyme cascade electrocatalysis; low background signal; DNA tetrahedron scaffold

INTRODUCTION

During the course of biological evolution in nature, the enzyme cascade reaction is an indispensable key step in signal transduction and amplification,[1-4] in which the catalytic efficiency mainly depends on the distance regulation of cooperating enzymes.[5-8] Specifically, the appropriate interenzyme distance could overcome intermediate decomposition, generate efficient mass transfer and increase local concentration of substrates, thereby resulting in high catalytic efficiency of enzyme cascade reaction.[9-13] Inspired by natural ingenuity, the method for increasing catalytic efficiency *via* regulating interenzyme distance of existing bioenzymes has been applied in the field of synthetic biology,[14] biomimicry[15-17] and biocatalysis[18-20]. However, its application in the construction of biosensors for electrochemical detection of biomolecules is confined by low sensitivity and limited detection limits, since an inevitable high electrochemical background signal is generated in the presence of existing bioenzymes and additional electron mediator.[21,22] Therefore, it is of critical importance to search a strategy which could not only reduce background signal but also enhance enzyme cascade catalytic efficiency simultaneously for the significant improvement of detection sensitivity of electrochemical biosensors.

To address the issue of high background signal, a rigid DNA tetrahedron (TDN) scaffold [23-28] was used to anchor glucose oxidase (GOx) at the vertex away from the electrode surface, in which a very low electrochemical signal was detected in the

absence of an electron mediator. Remarkably, only when the target thrombin and hemin were introduced, the hemin/G-quadruplex horseradish peroxidase-mimicking DNAzyme (HRP-mimicking DNAzyme) acting simultaneously as electrochemical signal probe would be formed at another vertex of TDN near the electrode surface, realizing the activation of high-efficiency enzyme cascade electrocatalysis with a desirable electrochemical response for target detection. Notably, by regulating the side length of TDN anchored HRP-mimicking DNAzyme and GOx at adjacent vertices, the optimal enzyme cascade electrocatalytic efficiency was acquired to further improve the detection sensitivity. As a proof of concept, this strategy of direct chemistry could not only avoid high background signal in the traditional cascade electrocatalysis of two existing bioenzymes, but also improve the enzyme cascade electrocatalytic efficiency simultaneously, thereby achieving the ultrasensitive electroanalytical detection of biomolecules.

In this work, an efficient target-activated enzyme cascade electrocatalysis with low background signal was applied to fabricate an ultrasensitive electrochemical biosensor for thrombin detection (as shown in Scheme 1). The rigid TDN scaffold carried two DNA fragments at adjacent vertices was self-assembled from four single-strand DNA, in which the gray pendant DNA fragment contained one-quarter of the G-quadruplex sequence (Scheme 1A). Afterwards, the DNA hairpin functionalized by glucose oxidase (GOx-primer) was complementary to the red DNA fragment of TDN, which allowed the GOx to be immobilized on the vertex of TDN scaffold (Scheme 1B). Subsequently, the Exo III-assisted target thrombin recycling amplification strategy was

introduced to generate massive DNA strands (output DNA) (Scheme 1C). The output DNA could not only open the DNA hairpin of GOx-primer including three-quarters of caged G-quadruplex sequence, but also synchronously capture the gray pendant DNA fragment at the vertex of TDN near the electrode surface to assemble hemin/G-quadruplex horseradish peroxidase-mimicking DNAzyme (HRP-mimicking DNAzyme) in the presence of hemin, which resulted in a desirable enzyme cascade electrocatalytic signal for thrombin quantitative detection(Scheme 1D). Notably, by regulating the side length of rigid TDN anchored HRP-mimicking DNAzyme and GOx at adjacent vertices, the optimal enzyme cascade electrocatalytic efficiency was obtained, which enabled further improvement of detection sensitivity. In summary, this strategy would provide new insights into ultrasensitive detection biomolecules in sensing analysis and disease diagnosis.

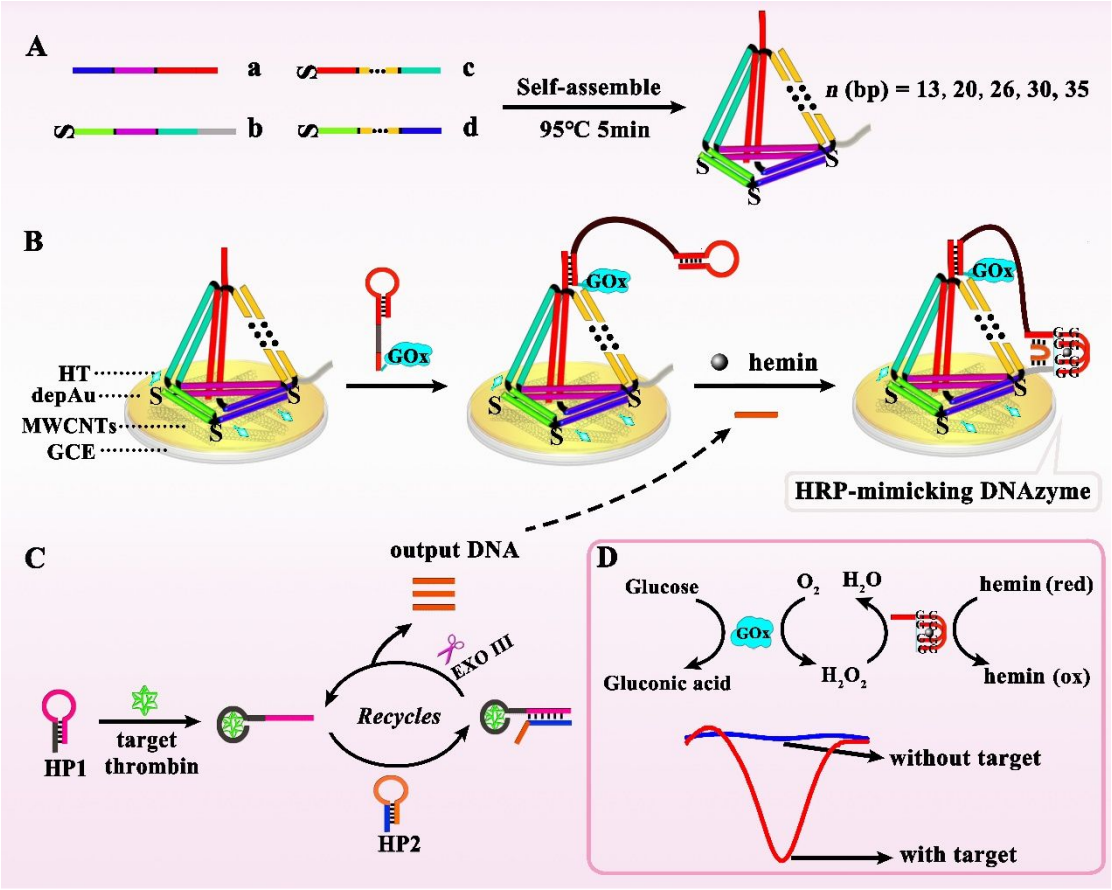

Scheme 1. Schematic illustration of (A) preparation of self-assembled TDN scaffolds for immobilization of model enzymes and regulation of interenzyme distance; (B) fabrication process of electrochemical biosensor based on an efficient target-activated enzyme cascade electrocatalysis; (C) Exo III-assisted target thrombin cycling amplification. (D) enzyme cascade electrocatalytic signal comparison of thrombin detection.

EXPERIMENTAL SECTION

Self-Assembly of the DNA Tetrahedron Scaffolds. To yield the DNA tetrahedron (TDN), equimolar quantities of four single-stranded DNA (a-d) were mixed in TM buffer (containing 50 mM DTT). Afterwards, this mixture was heated to 95 ºC for 5 min and immediately cooled down to 4 ºC within 30 s. Finally, the assembled TDN solution was stored in refrigerator at 4 °C for further use.

Preparation of Enzyme-Functionalized DNA primer. First, 50 μL of 5 μM freshly prepared GOx was activated with 20 mM SPDP for 1.5 h at 25 °C. Moreover, the thiolated DNA primer solution (2.5 μM) was incubated with 50 mM DTT for 2 hours at 25 °C to reduce S-S bonds. The superfluous DTT was removed by a centrifugal filter (Ultracel-30K membrane, Millipore). At last, the pretreated primer was further incubated with activated enzymes for 1.5 h at 25 °C to obtain enzyme-functionalized primer (GOx-primer).

Exo III-Assisted Autocatalytic Target Recycling Amplification Strategy. The elaborate steps were as follows: first, hairpin DNA HP1 containing thrombin binding aptamer was incubated with hairpin DNA HP2 and different concentrations of the target thrombin at 25 °C for 2 hours. Afterwards, 1.0 unit/μL of Exo III was added to the HP1-target-HP2 hybrid, followed by incubating for 40 min at 37 °C. Subsequently, the mixture was heated to 75 °C for 15 min to denature the Exo III enzymes and the final solution consisted of large numbers single-strand DNA (output DNA) was stored at 4 °C for further use.

RESULTS AND DISCUSSION

Characterization of DNA Nanostructures and depAu-MWCNTs. Native polyacrylamide gel electrophoresis (PAGE) was implemented to verify the formation of TDN nanostructure and GOx-primer. Figure 1A was the PAGE analysis for the self-assembled TDN. The lane 1-4 demonstrated the different single strand DNA (a-d), respectively. After four single strand DNA was assembled into TDN nanostructure, the bright band (lane 5) with slow electrophoretic mobility was clearly observed. Owing to

the most complex spatial structure and the largest molecular weight, the lane 6 posed a highest position, which demonstrated that the GOx-primer was linked to the TDN by DNA hybridization. In addition, the GOx-primer possessed a lower migration (lane 7) compared to that of the single strand DNA primer without GOx (lane 8), indicating the successful formation of GOx-primer. Moreover, we further employed fluid mode AFM (Figure 1B and Figure 1C) and TEM (Figure 1D) to verify the formation of the assembled TDN. In addition, the well-dispersed tubular structure, as displayed in Figure 1E, represented the typical scanning electron microscopy (SEM) images for the pristine MWCNTs. Moreover, compared to the initial MWCNTs, the bright clusters and spots appeared in Figure 1F, indicating that the electrodepositing enabled coverage of depAu on MWCNTs with large surface area.

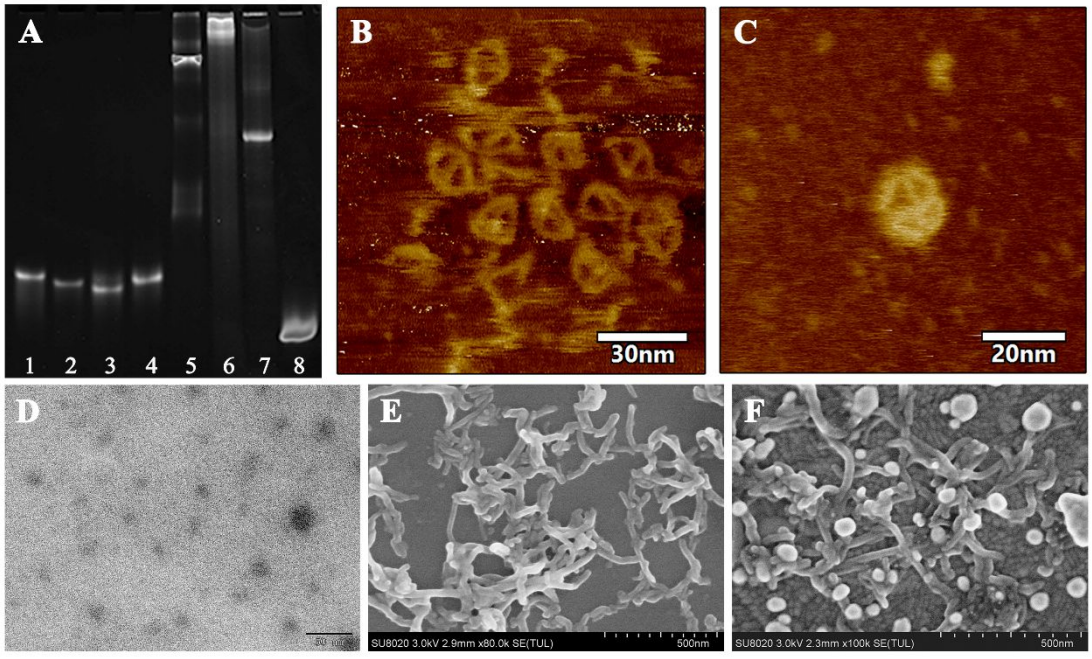

Figure 1. (A) PAGE characterization of the TDN and GOx-primer: lane 1, a; lane 2, c; lane 3, d; lane 4, b; lane 5, TDN; lane 6, TDN-GOx-primer; lane 7, GOx-primer; lane 8, primer. (B and C) AFM images and (D) TEM image of TDN. SEM images of (E) MWCNTs and (F) depAu-MWCNTs.

Verification of Enzyme Cascade Electrocatalytic Reaction. Control experimentation was implemented to investigate successful construction of high-efficiency enzyme cascade electrocatalysis. When the detection system contained TDN scaffold anchored GOx only (Figure 2A), a very low electrochemical response was detected. Moreover, the target-induced HRP-mimicking DNAzyme acting simultaneously as electrochemical signal probe was formed on the TDN scaffold without GOx (Figure 2B), an enhanced peak current was obtained owing to the direct electron transfer of HRP-mimicking DNAzyme. What's more, after GOx and HRP-mimicking DNAzyme were anchored at adjacent vertex of TDN scaffold, a highest electrochemical signal was observed (Figure 2C), suggesting that an effective enzyme cascade electrocatalytic reaction was activated successfully.

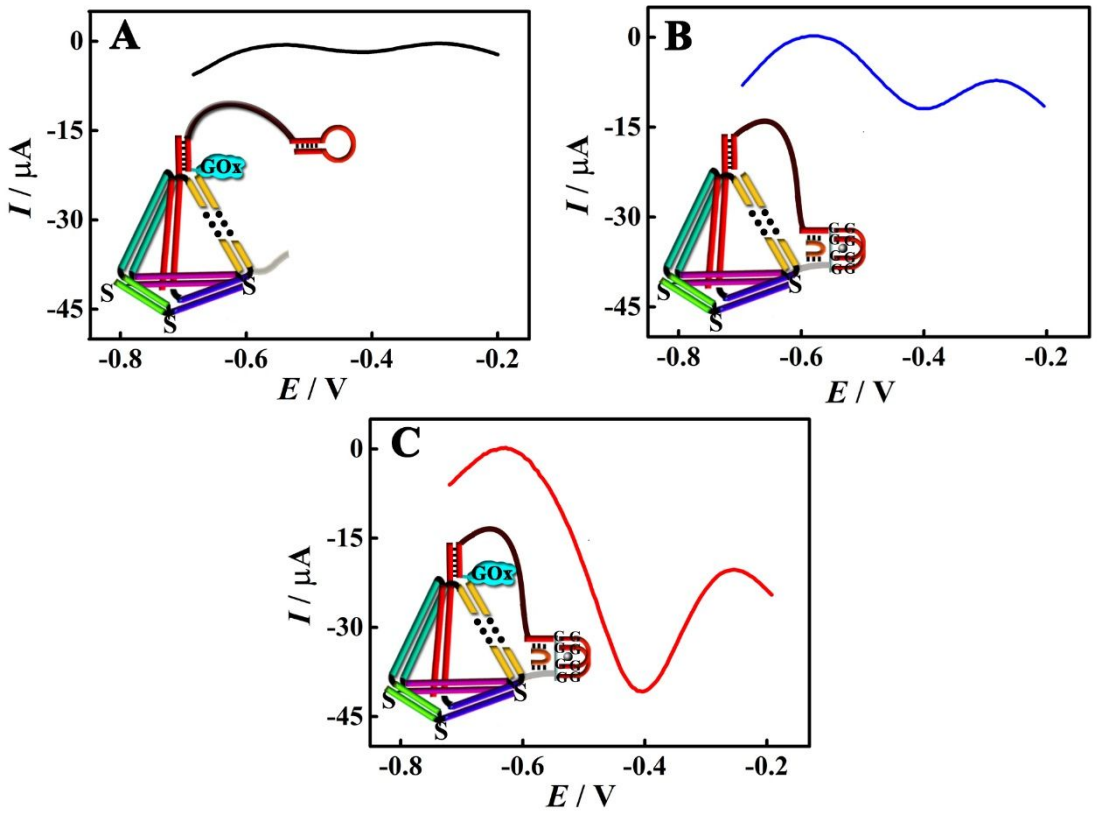

Figure 2. DPV responses of the biosensor containing TDN scaffold anchored (A) GOx only; (B)

HRP-mimicking DNAzyme only and (C) GOx and HRP-mimicking DNAzyme at adjacent vertex.

To further research the enzyme cascade electrocatalytic efficiency, as shown in Figure 3, we investigated the electrochemical responses of this biosensor without and with 5.0 mM glucose. In the present of glucose, electrochemical signal achieved obvious improvement in contrast to the absence of glucose, because the GOx catalyzed the oxidation of glucose to gluconic acid attached with reduction of O_2 to H_2O_2. Then, the resulting H_2O_2 formed a local high concentration around the hemin-G-quadruplex and subsequently was further reduced into H_2O with amplified electrochemical responses.

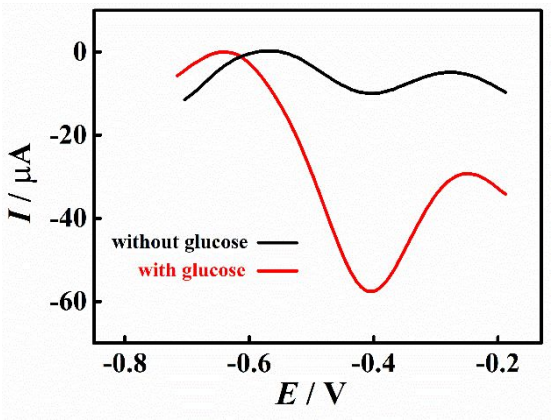

Figure 3. DPV responses of biosensor without and with glucose (5.0 mM) in the 0.1 M PBS solution (pH 7.0).

The Effect of Different Interenzyme Distance on Enzyme Cascade Electrocatalytic Efficiency. To certify that the enzyme cascade electrocatalytic efficiency relied on the interenzyme distance. The side length of rigid TDN anchored HRP-mimicking DNAzyme and GOx at adjacent vertices was ruled to systematically regulate interenzyme distance. As depicted in Figure 4, when the

side length of TDN increased from 13 bp to 20 bp, the DPV signal was gradually increased, which may be attributed to the avoidance of crowding effect to some extent. Additionally, with the side length of TDN increased from 30 bp to 35 bp, the electrocatalytic efficiency decreased due to the invalid diffusion of the intermediate product. Therefore, the TDN scaffold with the side edge length of 26 bp (approximately to 8.8 nm) was employed as the optimal interenzyme distance of GOx and HRP-mimicking DNAzyme for the highest catalytic efficiency.

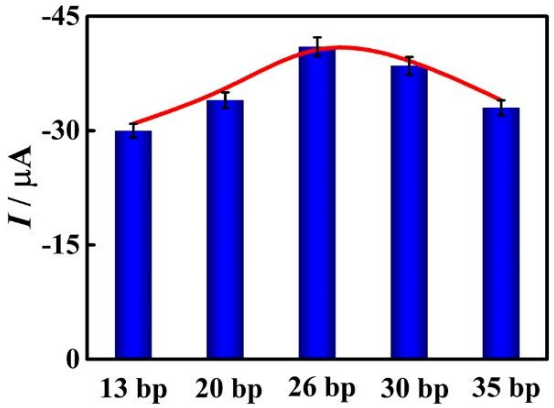

Figure 4. The effect of different interenzyme distance between HRP-mimicking DNAzyme and GOx on enzyme cascade electrocatalytic efficiency.

Performance of Proposed Biosensor. The potential quantitative application of the proposed platform was evaluated by DPV with different concentrations of thrombin under optimal conditions. The DPV peak current gradually increased with the concentration of thrombin increased from 1fM to 10 nM (Figure 5A). Furthermore, the DPV current responses and the logarithm of thrombin concentrations manifested a fine linear relationship (Figure 5B). The regression equation was I = -6.968 lg c_{target} - 26.80, and the limit of detection (LOD) for target detection was 0.3 fM. In addition, compared with some previous reports, as shown in Table S2, the proposed sensing system

achieved a superior sensitivity for thrombin detection owing to the application of efficient target-activated enzyme cascade electrocatalysis of HRP-mimicking DNAzyme and GOx, which reduced background signal significantly with optimal interenzyme distance.

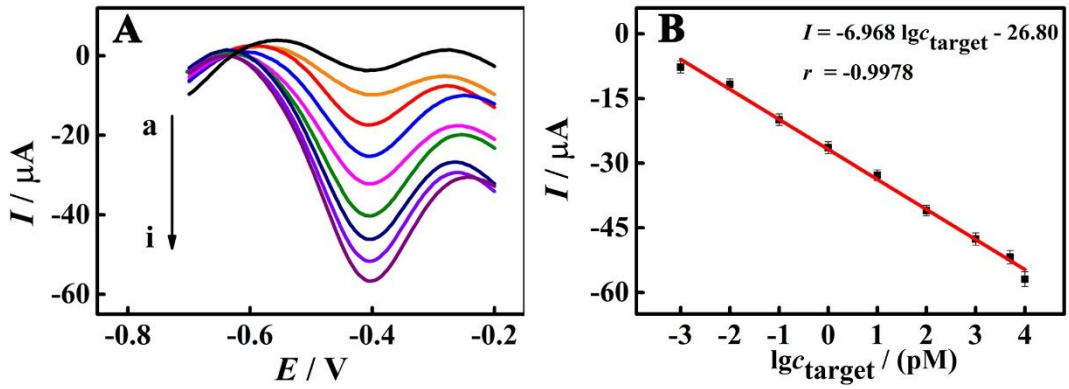

Figure 5. (A) DPV signals for various thrombin concentrations from a to i: 1 fM, 10 fM, 100 fM, 1 pM, 10 pM, 100 pM, 1 nM, 5 nM and 10 nM. (B) The calibration plot for thrombin.

Detection Specificity and Reproducibility. The specificity was investigated in the presence of several possible interfering proteins, such as hemoglobin (Hb), bovine serum albumin (BSA), carcinoembryonic antigen (CEA), prostate specific antigen (PSA) and α-1-fetoprotein (AFP). As depicted in Figure 6A, negligible electrochemical response was noticed for blank and interference proteins (10 nM), while the target thrombin at a concentration 100 times lower (0.1 nM) caused a significant current increase. Moreover, compared with the DPV response of thrombin (0.1 nM) only, the responses of the mixture containing the Hb, BSA, CEA, PSA, AFP and thrombin had no distinct change, manifesting the satisfactory selectivity of the biosensor exhibited towards thrombin. Additionally, five different batches of proposed biosensors were

applied to detect 0.1 nM target thrombin under the same conditions for assessing the reproducibility of the biosensor. As indicated from Figure 6B, the biosensors performed a similar electrochemical response with batch-to-batch relative standard deviation (RSD) of 3.27%. Moreover, 0.1 nM target thrombin was investigated by same biosensor for five times with RSD of 4.35%, indicating a favorable reproducibility of the proposed biosensor.

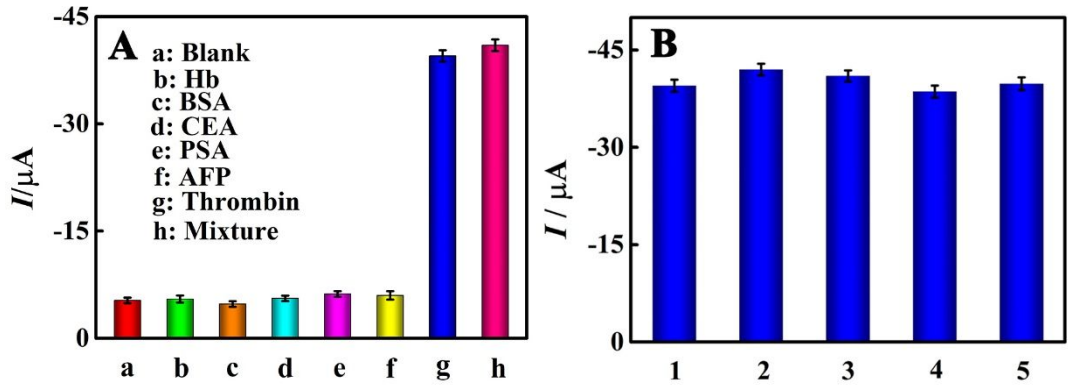

Figure 6. (A) Specificity of the electrochemical biosensors toward the blank control, Hb (10 nM), BSA (10 nM), CEA (10 nM), PSA (10 nM), AFP (10 nM), thrombin (0.1 nM), and the mixture (0.1 nM thrombin with 10 nM of Hb, BSA, CEA, PSA, and AFP, respectively). (B) Reproducibility of five different batches of the proposed biosensors.

Preliminary Application of the Electrochemical Biosensor. To evaluate the feasibility of fabricated sensor for real samples, different concentrations of spiked thrombin (10, 100, 1000 and 5000 pM) was added into healthy human serum (10-fold-diluted) to execute a recovery experiments. According to Table 1, the satisfactory recoveries was from 96.5% to 101.9% with relative standard deviation (RSD) between 2.28% and 5.04%, which denoted that the proposed sensor exhibited potential application in complex real samples.

Table 1. Detection of thrombin added in human serums (n = 3).

Sample number	Added/(pM)	Found/(pM)	Recovery/%	RSD/%
1	10	10.15	101.5	5.04
2	100	98.9	98.9	2.28
3	1000	1019.4	101.9	3.15
4	5000	4823.7	96.5	4.54

CONCLUSIONS

In summary, unlike the electrochemical biosensors based on traditional enzyme cascade reaction of two existing bioenzymes, the proposed biosensor containing target-activated enzyme cascade electrocatalysis of HRP-mimicking DNAzyme and GOx could offer the following advantages. First, only when the target thrombin was introduced, the HRP-mimicking DNAzyme would be generated to activate efficient enzyme cascade electrocatalysis, which could avoid the inevitable high background signal in traditional enzyme cascade reaction. Second, the target-induced HRP-mimicking DNAzyme acting simultaneously as electrochemical signal probe could avoid the introduction of additional electron mediator, making the detection system relatively simple and easy-operation. Third, the rigid TDN scaffold could not only anchor cascade enzymes at adjacent vertex efficiently, but also regulate interenzyme distance precisely, contributed to the acquisition of optimal enzyme cascade electrocatalytic efficiency for the further improvement of detection sensitivity. What's more, the described electrochemical biosensor realized the ultrasensitive detection of thrombin, which possessed great potential application for clinical diagnosis.

ASSOCIATED CONTENT

Supporting Information

Materials and reagents, apparatus and measurements, fabrication of the electrochemical biosensor, electrochemical characterization of the stepwise modified electrode, optimization of the experimental conditions, comparison of the proposed biosensor with other reported methods for thrombin detection (Table S2).

Notes

The authors declare no competing financial interests.

Acknowledgements

This work was financially supported by the NNSF of China (21775124, 21575116, 21675129, and 51473136), the Natural Science Foundation Project of CQ CSTC (cstc2018jcyjA0797), and the Fundamental Research Funds for the Central Universities (XDJK2018AA003, XDJK2019B022), China.

REFERENCES

(1) Kim, T. H.; Mehrabi, P.; Ren, Z.; Sljoka, A. Ing, C.; Bezginov, A.; Ye, L. B.; Pomes, R.; Prosser R. S.; Pai, E. F. *Science* **2017**, *355*, 2355.

(2) Krall, A. S.; Christofk, H. R. *Nature* **2017**, *546*, 357-358.

(3) Sweetlove, L. J.; Fernie, A. R. *Nat. Commun*. **2018**, *9*, 2136.

(4) Zhao, J.; Wang, S.; Lu, S.; Bao, X.; Sun, J.; Yang, X. *Anal. Chem*. **2018**, *90*, 7754-7760.

(5) Fu, J.; Yang, Y. R.; Johnson-Buck, A.; Liu, M.; Liu, Y.; Walter, N. G.; Woodbury, N. W.; Yan, H. *Nat. Nanotechnol*. **2014**, *9*, 531-536.

(6) Wheeldon, I.; Minteer, S. D.; Banta, S.; Barton, S. C.; Atanassov, P.; Sigman, M. *Nat. Chem*. **2016**, *8*, 299-309.

(7) Sun, L.; Gao, Y. J.; Xu, Y.; Chao, J.; Liu, H. J.; Wang, L. H.; Li, D.; Fan, C. H. *J. Am. Chem. Soc*. **2017**, *139*, 17525-17532.

(8) Fu, J.; Liu, M.; Liu, Y.; Woodbury, N. W.; Yan, H. *J. Am. Chem. Soc*. **2012**, *134*, 5516-5519.

(9) Zhao, X.; Palacci, H.; Yadav, V.; Spiering, M. M.; Gilson, M. K.; Butler, P. J.; Hess, H.; Benkovic, S. J.; Sen, A. *Nat. Chem*. **2018**, *10*, 311-317.

(10) Ngo, T. A.; Nakata, E.; Saimura, M.; Morii, T. *J. Am. Chem. Soc*. **2016**, *138*, 3012-3021.

(11) Tsitkov, S.; Hess, H. *ACS Catal.* **2019**, *9*, 2432-2439.

(12) Feng, D. W.; Liu, T. F.; Su, J.; Bosch, M.; Wei, Z. W.; Wan, W.; Yuan, D. Q.; Chen, Y. P.; Wang, X.; Wang, K. C.; Lian, X. Z.; Gu, Z. Y.; Park, J.; Zou, X. D.; Zhou, H. C. *Nat. Commun*. **2015**, *6*, 5979.

(13) Zhao, M. T.; Deng, K.; He, L. C.; Liu, Y.; Li, G. D.; Zhao, H. J.; Tang, Z. Y. *J. Am. Chem. Soc*. **2014**, *136*,1738-1741.

(14) Chen, Y. H.; Ke, G. L.; Ma, Y. L.; Zhu, Z.; Liu, M. H.; Liu, Y.; Yan, H.; Yang, C. J. *J. Am. Chem. Soc*. **2018**, *140*, 8990-8996

(15) Chen, G.; Huang, S.; Kou, X.; Wei, S.; Huang, S.; Jiang, S., Shen, J., Zhu, F., Ouyang, G. *Angew. Chem. Int. Ed*. **2019**, *58*, 1463-1467.

(16) Mukai, C.; Gao, L.; Nelson, J. L.; Lata, J. P.; Cohen, R.; Wu, L.; Hinchman, M. M.; Bergkvist, M.; Sherwood, R. W.; Zhang, S.; Travis, A. J. *Angew. Chem. Int. Ed*. **2017**, *56*, 235-238.

(17) Wang, H.; Zhao, Z.; Liu, Y. X.; Shao, C. M.; Bian, F. K.; Zhao, Y. J. *Sci. Adv*. **2018**, *4*, 2816.

(18) Chen, W. H.; Vázquez-González, M.; Zoabi, A.; Abu-Reziq, R.; Willner, I. *Nat. Catal*. **2018**, *1*, 689-695.

(19) Ke, G.; Liu, M.; Jiang, S.; Qi, X.; Yang, Y. R.; Wootten, S.; Zhang, F.; Zhu, Z.; Liu, Y.; Yang; C. J.; Yan, H. *Angew. Chem. Int. Ed*. **2016**, *55*, 7483-7486.

(20) Hwang, E. T.; Lee, S. *ACS Catal*. **2019**, *9*, 4402-4425.

(21) Kou, B. B.; Chai, Y. Q.; Yuan, Y. L.; Yuan, R. *Anal. Chem*. **2018**, *90*, 10701-10706.

(22) Wang, D.; Chai, Y. Q.; Yuan, Y. L.; Yuan, R. *Anal. Chem*. **2019**, *91*, 3561-3566.

(23) Li, C.; Hu, X. L.; Lu, J. Y.; Mao, X. X.; Xiang, Y.; Shu, Y. Q.; Li, G. X. *Chem. Sci*. **2018,** *9*, 979-984.

(24) Wan, Y.; Zhu, N. H.; Lu, Y.; Wong, P. K. *Anal. Chem*. **2019**, *91*, 2626-2633.

(25) Liu, Q.; Ge, Z.; Mao, X.; Zhou, G.; Zuo, X.; Shen, J.; Shi, J.; Li, J.; Wang, L.; Chen; X.; Fan, C. *Angew. Chem. Int. Ed.* **2018**, *57*, 7131-7135.

(26) Nie, W. Y.; Wang, Q.; Zou, L. Y.; Zheng, Y.; Liu, X. F.; Yang, X. H.; Wang, K. M. *Anal. Chem*. **2018**, *90*, 12584-12591.

(27) Lin, M.; Wang, J.; Zhou, G.; Wang, J., Wu, N., Lu, J., Gao, J., Chen, X., Shi, J., Zuo, X., Fan, C. *Angew. Chem. Int. Ed.* **2015**, *54*, 2151-2155.

(28) Lin, Y.; Jia, J. P.; Yang, R.; Chen, D. Z.; Wang, J.; Luo, F.; Guo, L. H.; Qiu, B.; Lin, Z. Y. *Anal. Chem*. **2019**, *91*, 3717-3724.

For TOC only

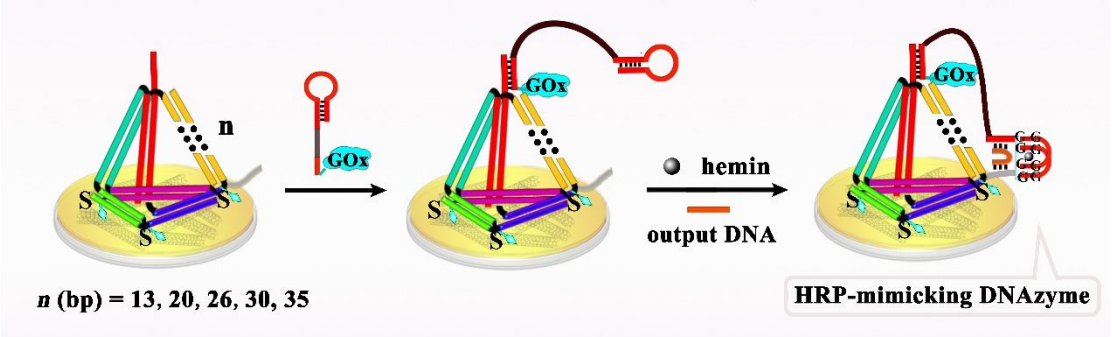
n
GOx
GOx
hemin
output DNA
GOx
n (bp) = 13, 20, 26, 30, 35
HRP-mimicking DNAzyme